L. Mourokh, P. Ivanushkin, Y. Yoon, N. Aoki, Y. Ochiai et al.

Related Articles

Protocols for characterising quantum transport through nano-structures
Appl. Phys. Lett. 101, 133106 (2012)

Electrical modulation of the edge channel transport in topological insulators coupled to ferromagnetic leads
J. Appl. Phys. 112, 063710 (2012)

Interplay of magnetic field and geometry in magneto-transport of mesoscopic loops with Rashba and Dresselhaus spin-orbit interactions
J. Appl. Phys. 112, 024321 (2012)

Spin resolved conductance in semiconductor mesoscopic rings: not spin gate response
J. Appl. Phys. 111, 124502 (2012)

Aharonov-Bohm effect in an electron-hole graphene ring system
Appl. Phys. Lett. 100, 203114 (2012)

Additional information on J. Appl. Phys.

Journal Homepage: http://jap.aip.org/
Journal Information: http://jap.aip.org/about/about_the_journal
Top downloads: http://jap.aip.org/features/most_downloaded
Information for Authors: http://jap.aip.org/authors

Multi-continuum Fano resonance in coupled quantum point contacts: A manifestation of the "integral" Fano formula

L. Mourokh,[1] P. Ivanushkin,[1] Y. Yoon,[2] N. Aoki (青木伸之),[3] Y. Ochiai (落合勇一),[3] and J. P. Bird[2,3]

[1]*Physics Department, Queens College of CUNY, 65-30 Kissena Blvd., Flushing, New York 11367, USA*
[2]*Department of Electrical Engineering, University at Buffalo, Buffalo, New York 14260, USA*
[3]*Graduate School of Advanced Integration Science, Chiba University, 1-33 Yayoi-cho, Inage-ku, Chiba 263-8522, Japan*

We discuss how a pair of quantum point contacts (QPCs), which are coupled to each other via their mutual wavefunction overlap with a common continuum, can be used to provide a realization of a *multi-continuum* Fano resonance. This behavior arises from the multi-subband character of the QPCs, each of whose transverse subbands may be viewed as providing a unique continuum. Reminiscent of the original analysis of Fano, we show that the resonance exhibited by this system can be defined in terms of an asymmetry parameter (q) and characteristic level broadenings (Γ & Γ_0), although these parameters now determine the resonance lineshape through their inclusion in energy integrals, a result that we refer to as the "integral" Fano formula. We also demonstrate how, dependent upon the effective dimensionality of the "detector" QPC that exhibits the Fano resonance, the resonance amplitude can significantly exceed the one-dimensional conductance quantum ($2e^2/h$). Our experimental and theoretical results, therefore, provide further support for the scenario of spontaneous bound-state formation in QPCs near pinch-off and suggest that this bound state may be used to study new aspects of Fano-resonance phenomenology. © *2012 American Institute of Physics.* [http://dx.doi.org/10.1063/1.4765026]

I. INTRODUCTION

The Fano resonance[1] is a quantum-mechanical interference phenomenon that arises when a transition to a final state occurs simultaneously via a continuum and a discrete quantum level. Although this phenomenon was originally discussed in relation to photoionization in atomic physics,[1] it has subsequently been observed in various atomic,[2,3] optical,[4,5] and mesoscopic systems.[6–8] (For a recent review of Fano resonances in mesoscopic systems, we refer the reader to Ref. 9, while Ref. 10 contains some more general comments on this phenomenon.) When the discrete state involved in the resonance process has energy E_0 and width Γ, Fano showed that the resonance cross-section is given by

$$\sigma = \sigma_0 \frac{(\varepsilon + q)^2}{\varepsilon^2 + 1}, \tag{1}$$

where $\varepsilon = (E - E_0)/\Gamma$ is the detuning from the resonance level and q is the Fano parameter that characterizes the asymmetry of the resonance lineshape. The two limiting cases of Fano resonances are a symmetric Breit-Wigner resonance ($|q| = \infty$), when the transition from the continuum is vanishingly weak, and; a symmetric anti-resonance (dip) for $q = 0$ when the continuum transition dominates. In all other cases, the resonance lineshape is asymmetric, with $q = 1$ yielding maximal asymmetry and corresponding to the situation where transmission via the continuum and discrete level are of the same amplitude.

In solid-state realizations of the Fano resonance, it is common to implement the discrete level by making use of

gated quantum dots.[6–8] In these structures, however, the transfer matrix element between the dot and the continuum is typically small. In order to increase it, it is therefore necessary to physically implement the continuum (formed by a Fermi sea of conduction electrons) in close proximity to the dot, which has the unintended consequence of also increasing the Coulomb interaction.[8] We have recently demonstrated an alternative implementation of Fano resonances, however, by exploiting the phenomenon of bound-state (BS) formation in quantum point contacts (QPCs) near pinch-off. While this phenomenon was first predicted in Refs. 11 and 12, it has subsequently been confirmed in a number of other theoretical reports, each of which start from different initial assumptions yet nonetheless arrive at the same conclusion regarding the existence of such a BS.[13–15] To achieve experimental detection of this BS, we have performed experiments on pairs of QPCs, which we couple non-locally by means of a high-mobility two-dimensional electron gas (2DEG).[16–19] The continuum required for the Fano resonance is then provided by a "detector" QPC, which we configure far away from pinch-off, while the bound state is formed in a "swept" QPC. In a series of experiments[16–19] and associated theoretical reports,[20,21] we have shown that a Fano resonance is observed in the conductance of the detector-QPC, when the BS formed in the swept-QPC is driven up through the Fermi level at pinch-off. In Ref. 18, we demonstrated that the lineshape of this resonance could be varied systematically in experiment, simply by changing the distance between the two QPCs, thereby affecting the discrete-state/continuum coupling that governs the Fano resonance.

While the study of Fano resonances has a long history, more than half a century, by far the vast majority of studies have focused on the interference arising by coupling a single continuum to just one discrete level. In his original analysis, however, Fano also predicted[1] the possibility of more-complicated resonances, involving either the interference of a single level with multiple continua or the coupling of multiple discrete states to a common continuum. Recently, we have realized a demonstration of the latter *multi-state* Fano resonance, by forming two bound states on separate QPCs, and coupling these to each other (and a detector) via a region of 2DEG.[22] Another distinctive feature of QPCs, however, is that they may easily be configured to carry a current via a number of one-dimensional subbands. Since each one of these subbands may be viewed as representing a particular continuum, in this report we discuss how our experimental setup also provides a natural footing to implement a *multi-continuum* Fano resonance. Specifically, we demonstrate how appropriate configuration of the detector-QPC can cause it to exhibit a Fano resonance with an amplitude that significantly exceeds $2e^2/h$ ($\equiv G_0$), thereby providing a clear indication that more than one subband participates in the resonance. We confirm this result by calculating the conductance of a multi-subband detector-QPC that is coupled to a BS. Starting from the transfer Hamiltonian for a single subband, we derive equations of motion for electron operators and determine the Green's functions for the detector and BS electrons, as well as their dependence on the system parameters. We thus show that the current (and the conductance) of the detector exhibits a clear Fano resonance. Unlike usual discussions of such resonances, however, its q-parameter and linewidth appear in integrations over the electron energy in the detector and reservoirs, a result that we refer to as the "integral" Fano formula. To provide a straightforward generalization of this formula to the multi-subband case, we neglect the role of subband mixing in the detector and obtain its total conductance, as well as the amplitude of its resonant peak, by simple superposition of the contributions from each continuum (i.e., from each subband). While we show here that this approach accurately predicts the giant Fano resonances observed in experiment, we caution that in strongly nonlinear situations (in particular, at high source-drain voltages), the underlying physics may be more complicated. This will need to be addressed in future work, however.

II. EXPERIMENTAL RESULTS

The experiments reported here were performed on the multi-gate device of Refs. 17–19 (Fig. 1(a)), which was realized in a GaAs/AlGaAs 2DEG of density 2.3×10^{11} cm^{-2}, mobility 4×10^6 cm^2/Vs, Fermi wavelength 53 nm, and mean free path 31 microns (at 4.2 K, where all measurements reported here were performed). A scanning-microscope image of the device is shown in Fig. 1(a), on which we also indicate schematically the ohmic and gate contacts that were formed on the device mesa. These contacts allowed us to independently determine the conductance of the various QPCs and to demonstrate a Fano resonance in the conductance of a detector-QPC when configured close to a swept-QPC that is
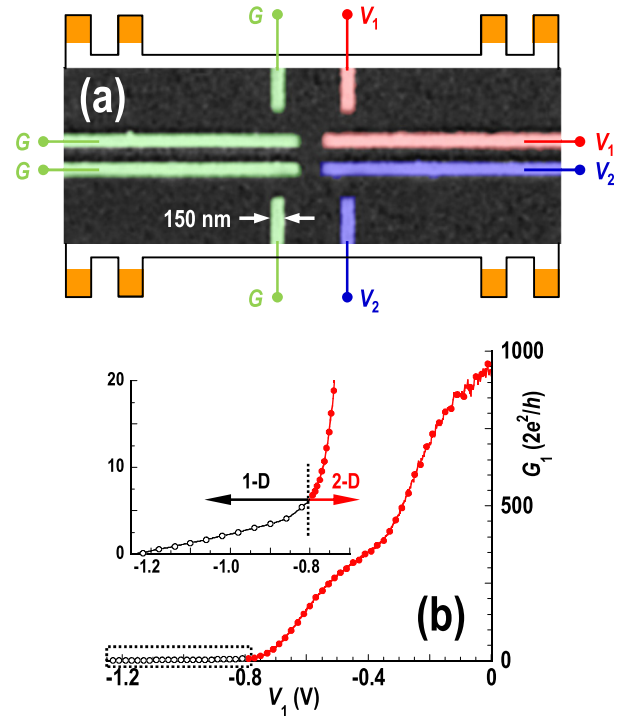

FIG. 1. (a) Colorized scanning-electron micrograph of the device used to implement the coupled QPCs in this study. Gates whose terminals are denoted by "*G*" are held at ground potential in the experiments and so do not influence the 2DEG underneath them. The gates biased with the voltage V_1/V_2 form the detector-/swept QPC. This figure also illustrates schematically the eight Ohmic contacts that could be used to make measurements in various probe configurations. (b) Measured variation of the conductance (G_1) of the detector QPC as a function of its gate voltage (V_1) at 4.2 K. Data plotted with filled, and open, symbols are referred to here as the 2-D, and 1-D, regimes, respectively. The inset shows an expanded view of the region enclosed by the dotted lines in the main panel. For clarity, not all data points are plotted.

driven to pinch-off. Although we focus here on results obtained for a particular device, we emphasize that this device contains multiple (6) QPCs, each of which allowed observation of the resonance when used as either the swept- or control-QPC.[17] Moreover, the resonance phenomenon that we discuss has been observed in multiple thermal cycles performed over a period of three years, in devices fabricated on other wafers, and for coupled QPCs with different gate geometries.[16,17]

To illustrate the key points of interest here, we focus on measurements obtained for the configuration shown in Fig. 1(a), in which a voltage V_1 is applied to the upper right-hand pair of gates to form the detector-QPC, while the lower right-hand pair form the swept-QPC that is biased at gate voltage V_2. The left-hand set of gates, as denoted by "*G*," is held at ground potential and so have no significant influence on the underlying 2DEG. We emphasize again that the results obtained for this gate configuration should be considered as illustrative, and are reproduced in measurements of other configurations. In Fig. 1(b), we plot the measured conductance ($G_1(V_1)$) of the detector-QPC as a function of its gate voltage (V_1). As indicated by the filled and open data points, the results of this single measurement can be broken up into two characteristic gate-voltage ranges. The first of these (filled symbols) is characterized by a rapid change of G_1 with V_1, while the second (open

symbols) corresponds to a much slower variation. Physically, the former range corresponds to the situation where the 2DEG directly underneath the gates is still not fully depleted, and so the detector-QPC is not formed. In this regime, which we refer to hereafter as the two-dimensional (2-D) regime, the detector device is essentially of 2-D character. The latter range, on the other hand, should correspond to the situation where the QPC is formed and the detector exhibits its 1-D character. (It should be noted here that, due to our relatively-high measurement temperature of 4.2 K, the 1-D conductance quantization is not resolved.[17] This can be attributed to thermal smearing of the Fermi level[23] and is properly accounted for in our theory below.) The inset to Fig. 1(b) shows an expanded view of the region enclosed by dotted lines in the main panel and indicates that the transition between the 2-D and 1-D regimes occurs near $V_1 = -0.8$ V. Simply by variation of V_1, we should therefore be able to study the influence of the effective dimensionality of the detector on its Fano resonance, and it is this issue that provides a focus of this manuscript.

In Fig. 2, we show as insets examples of the Fano resonance exhibited in the conductance of the detector-QPC and thus highlight the manner in which this resonance is modified by varying the detector conductance. The main panel plots the data of Fig. 1(b), this time showing the variation of $G_1(V_1)$ on a logarithmic scale. Referring to the insets, panel ⑤ shows a small resonance, with an amplitude of
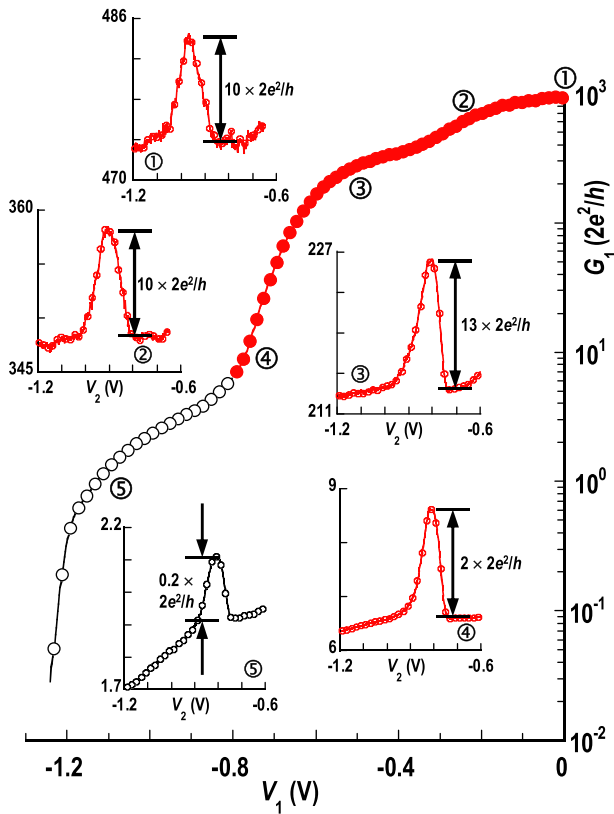
around $0.2G_0$, when the detector is configured in the 1-D regime of Fig. 1(b). As we have reported previously, this resonance is correlated to the pinch-off of the swept-QPC (not shown here), and its amplitude of $<G_0$ is also typical of our prior experiments.[16–19] Of more interest is the behavior exhibited in panels ①–④, which show that a resonance with an amplitude very much larger than G_0 can be obtained by configuring the detector in its "2-D" regime. Indeed, panel ① corresponds to the case $V_1 = 0$, for which there is no detector-QPC as such and the role of the detector is instead provided by a macroscopic region of 2DEG. In spite of this, we see a detector resonance with an amplitude of around $10G_0$, and a peak of similar magnitude is also apparent in panels ② and ③. Only as we make V_1 more negative and approach the "1-D" detector regime, do we see a reduction in the resonance amplitude, as indicated by panels ④ and ⑤. A major focus of the remainder of this paper will, therefore, be on explaining our observation of a detector resonance with an amplitude either much greater, or smaller, than G_0, dependent upon the effective detector dimensionality.

III. FANO-RESONANCE OF COUPLED QUANTUM POINT CONTACTS: THEORETICAL FORMULATION FOR A SINGLE-SUBBAND DETECTOR

To account for our experimental observations, we first examine the conductance of a single-subband QPC (representing our detector) that is formed between a pair of 2DEG reservoirs, and which is coupled via mutual wavefunction overlap to a BS of energy E_0. As demonstrated previously in Ref. 20, this kind of model system provides a useful means to describe the detector-BS coupling. In this work, we start from the Hamiltonian:

$$H = \sum_{k_{QPC}} E_{k_{QPC}} a^+_{k_{QPC}} a_{k_{QPC}} + \sum_{k_L} E_{k_L} c^+_{k_L} c_{k_L} + \sum_{k_R} E_{k_R} c^+_{k_R} c_{k_R}$$

$$+ E_0 a^+_0 a_0 + \sum_{k_L k_{QPC}} \left(T_{k_L k_{QPC}} c^+_{k_L} a_{k_{QPC}} + T^*_{k_L k_{QPC}} a^+_{k_{QPC}} c_{k_L} \right)$$

$$+ \sum_{k_R k_{QPC}} \left(T_{k_R k_{QPC}} c^+_{k_R} a_{k_{QPC}} + T^*_{k_R k_{QPC}} a^+_{k_{QPC}} c_{k_R} \right)$$

$$+ \sum_{k_{QPC}} \left(V_{k_{QPC}} a^+_{k_{QPC}} a_0 + V^*_{k_{QPC}} a^+_0 a_{k_{QPC}} \right), \quad (2)$$

where $a^+_{k_{QPC}}/a_{k_{QPC}}$, $c^+_{k_{L,R}}/c_{k_{L,R}}$, and a^+_0/a_0 are, respectively, electron creation/annihilation operators for the QPC, the left (L) and right (R) reservoirs, and the BS. The energies $E_{k_{QPC}}$ and $E_{k_{L/R}}$ are for electrons with wavenumber k in the QPC, and the left and right reservoirs, respectively. The matrix element $T_{k_{L,R} k_{QPC}}$ describes electron transfer between the QPC and the reservoirs, while $V_{k_{QPC}}$ describes that between the QPC and the BS. It is this latter matrix element that therefore provides the effective coupling between the detector and the BS.

We next derive the Heisenberg equations of motion for the electron operators and obtain corresponding Green's functions. The Fourier transform for the Green's function of the QPC electrons takes the form:

FIG. 2. The main panel re-plots the data of Fig. 1(b), this time with G_1 plotted on a logarithmic axis. Insets show the detector peak observed in G_1 as the swept-QPC is driven to pinch-off (also at 4.2 K, see Refs. 17–19 for further details). The five different panels plotted as insets correspond to different values of the detector conductance, as indicated by the labeling in the main figure.

$$G_{k_{QPC}}(\omega) = (\omega - E_{k_{QPC}} - i\Gamma_R(\omega) - i\Gamma_L(\omega))^{-1}, \quad (3)$$

where we have neglected any energy shift due to the reservoir-QPC interaction. The level broadenings due to this interaction are determined from the imaginary parts of the reservoir Green's functions:

$$\Gamma_{L,R}(\omega) = \sum_{k_{L,R}} \left| T_{k_{L,R}k_{QPC}} \right|^2 \text{Im } g_{k_{L,R}}^r(\omega), \quad (4)$$

with

$$\text{Im } g_{k_{L,R}}^r(\omega) = \pi\delta(\omega - E_{k_{L,R}}). \quad (5)$$

The Green's function of the BS electrons is given by

$$G_0(\omega) = (\omega - E_0 - i\Gamma_0(\omega))^{-1} \quad (6)$$

and, by considering a symmetric QPC ($\Gamma_L = \Gamma_R = \Gamma/2$), the broadening of the BS can be expressed as

$$\Gamma_0(\omega) = \sum_{k_{QPC}} \left| V_{k_{QPC}} \right|^2 \text{Im } G_{k_{QPC}}(\omega)$$
$$= \sum_{k_{QPC}} \left| V_{k_{QPC}} \right|^2 \frac{\Gamma(\omega)}{(\omega - E_{k_{QPC}})^2 + \Gamma^2(\omega)}. \quad (7)$$

An explicit expression for the broadening Γ can be obtained by using a relation connecting the transfer matrix element of the QPC with its transmission coefficient ($\tilde{T}$), and the densities of states in both sides in the reservoirs (D_{2D}) and the QPC (D_{QPC}).[23] This relation takes the form:

$$\left| T_{k_{2D}k_{QPC}} \right|^2 = \frac{\tilde{T}}{2\pi^2 D_{2D}D_{QPC}}. \quad (8)$$

By substituting Eqs. (5) and (8) into Eq. (4) and replacing the summation with an integration as

$$\sum_{k_{2D}}(...) \rightarrow \int dE_{k_{2D}}D_{2D}(...), \quad (9)$$

where $dE_{k_{2D}}$ is used for both reservoirs, we obtain the desired broadening as

$$\Gamma(E) = \frac{\tilde{T}}{\pi D_{QPC}}. \quad (10)$$

The physical significance of this parameter becomes clearer, if one has full transmissions at the boundaries, $\tilde{T} = 1$, and a one-dimensional density of states for the n-th subband of the QPC in the form:

$$D_{QPC}^{1D} = \frac{1}{\pi\hbar} \left(\frac{m^*}{2} \right)^{1/2} (E - E_n)^{-1/2}L, \quad (11)$$

where m^* is the electron effective mass, L is the length of the structure, and E_n is the bottom of the subband. In this case, the broadening can be written as

$$\Gamma(E) = \frac{\hbar}{L} \left(\frac{2(E - E_n)}{m^*} \right)^{1/2} = \frac{\hbar}{\tau}, \quad (12)$$

where τ is the transfer time defined as

$$\tau = \frac{L}{v} = L \left(\frac{2(E - E_n)}{m^*} \right)^{-1/2}, \quad (13)$$

with v being the electron velocity along the QPC direction. According to this result, the broadening of Eq. (10) can be understood as arising from the finite lifetime of electrons inside the QPC region.

IV. THE ELECTRON CURRENT AND THE "INTEGRAL" FANO FORMULA

Next, we calculate the electron current through the QPC, which we write as

$$I = I_L = e\frac{d}{dt} \sum_{k_L} \langle c_{k_L}^+ c_{k_L} \rangle$$
$$= \frac{ie}{\hbar} \sum_{k_L, k_{QPC}} (T_{k_L k_{QPC}} \langle c_{k_L}^+ a_{QPC} \rangle - T_{k_L k_{QPC}}^* \langle a_{QPC}^+ c_{k_L} \rangle). \quad (14)$$

We evaluate this expression using the Langreth theorem,[24] and the Green's functions determined in Sec. III. After replacing the summation with an integration (as in Eq. (9)), we then obtain

$$I = \frac{e}{h}\frac{\tilde{T}}{\pi} \int dE_{k_{2D}} \int dE_{k_{QPC}}[f_L(E_{k_{2D}}) - f_R(E_{k_{2D}})]\text{Im } G_{k_{QPC}}(E_{k_{2D}})$$
$$\times \left(1 + \Gamma_0(E_{k_{2D}}) \left[\frac{\text{Re}^2 G_{k_{QPC}}(E_{k_{2D}})}{\text{Im}^2 G_{k_{QPC}}(E_{k_{2D}})} \text{Im } G_0(E_{k_{2D}}) \right.\right.$$
$$\left.\left. + 2\frac{\text{Re} G_{k_{QPC}}(E_{k_{2D}})}{\text{Im } G_{k_{QPC}}(E_{k_{2D}})} \text{Im } G_0(E_{k_{2D}}) - \text{Im } G_0(E_{k_{2D}}) \right] \right), \quad (15)$$

where the Fermi functions of electrons in the left and right reservoirs are defined as $f_L(E_{k_{2D}}) = (\exp\{(E_{k_{2D}} - E_F - V/2)/T\} + 1)^{-1}$ and $f_R(E_{k_{2D}}) = (\exp\{(E_{k_{2D}} - E_F + V/2)/T\} + 1)^{-1}$, respectively, with V being the applied source-drain voltage (we express temperature, energy, frequency, and voltage in units of eV). Following Refs. 1 and 25, we introduce the parameters:

$$q = \frac{\text{Re} G_{k_{QPC}}}{\text{Im } G_{k_{QPC}}} = \frac{E_{k_{2D}} - E_{k_{QPC}}}{\Gamma} \quad (16)$$

and

$$\varepsilon = \frac{E_{k_{2D}} - E_0}{\Gamma_0}, \quad (17)$$

to finally obtain

$$I = \frac{e}{h}\tilde{T} \int dE_{k_{2D}}[f_L(E_{k_{2D}})$$
$$- f_R(E_{k_{2D}})] \int dE_{k_{QPC}}D_{QPC}(E_{k_{QPC}})\frac{1}{1 + q^2}\frac{(\varepsilon + q)^2}{\varepsilon^2 + 1}. \quad (18)$$

On comparing Eq. (18) to the standard Landauer formula, it is evident that the transmission coefficient has the Fano line-shape of Eq. (1), normalized by the factor $1/(1+q^2)$. A key difference with the standard Fano resonance, furthermore, is that both ε and q are now functions of the integration variables, for which reason we refer to Eq. (18) the "integral" Fano formula.

While Eq. (18) was derived for a single-subband QPC, its generalization to the multi-subband case is quite straightforward if inter-subband scattering is negligible, which should be valid for the extremely clean samples used in our experiments. Under this condition, an additional summation over all subbands should be added to the QPC density of states (D_{QPC}), the bound-state broadening (Γ_0, see Eq.(7)), and the expression for the QPC current (Eq. (18)). In general, the two electron spin projections should be considered as independent continua, but in the present, spin-degenerate, case they are accounted for simply by multiplying the calculated contribution of each subband to the current by a factor of two.

V. THEORETICAL RESULTS

The conductance ($G = I/V$) obtained from Eq. (18) for the QPC/BS system is shown in Fig. 3 as a function of the energy separation between the Fermi level (E_F) and the BS. A word is merited at this point, on the correspondence of these calculations to the results of experiment, in which the BS is formed in the swept-QPC.[16–19] As the voltage (V_2) applied to the gates of this QPC are made more negative, the confinement of its BS should be increased, thereby driving it up through E_F. The detuning shown on the horizontal axis of Figs. 3(a)–3(d) should therefore be viewed as being proportional to V_2, with
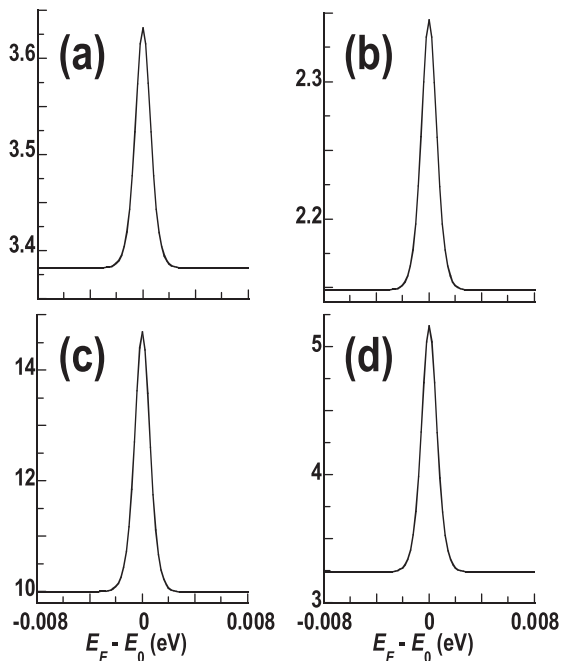

FIG. 3. QPC conductance calculated at 4.2 K, as a function of the energy detuning between the Fermi energy and the discrete state (with energy E_0). (a) and (b) assume a 1-D density of states for the QPC, while (c) and (d) assume a 2-D one. (a) $\hbar\omega = 3$ meV, (b) $\hbar\omega = 4.5$ meV, (c) $\hbar\omega = 1$ meV, (d) $\hbar\omega = 3$ meV.

$E_F - E_0$ increasing as this voltage is made more negative. To obtain the results shown in Fig. 3, we consider an equidistant set of QPC subbands with minimal subband energies $E_n = (n + {}^1/_2)\hbar\omega$, $n = 0, 1, 2,\ldots$. To provide a direct comparison to the results of our experiment in Sec. II, in all calculations, we take $E_F = 10$ meV, $V = 0.5$ mV, and $T = 4.2$ K. For ballistic transport through the QPC, we can take $\tilde{T} = 1$, so that we then use $|V_{kQPC}|^2 = 5 \times 10^{-12}$ (eV)^2 as the *only* fitting parameter. It should therefore be emphasized that the fitting we perform using this parameter essentially provides us with a means to determine V_{kQPC} from experiment, something that was not possible previously but which is important due to the fact that this parameter indicates the strength of the coupling between the detector and the BS.

Turning to our results, in Figs. 3(a) and 3(b), we consider a 1-D density of states of Eq. (11) for the QPC, ($m^* = 0.067m_0$, with m_0 the free-electron mass, and $L = 100$ nm). In Figs. 3(c) and 3(d), in contrast, we have used a two-dimensional form for the detector density of states:

$$D_{QPC}^{2D} = \frac{m^*}{\pi\hbar^2} LW, \tag{19}$$

with $W = 100$ nm being the approximate distance between the gates. It should also be emphasized that the linewidths, Γ and Γ_0, are not parameters, but functions, and are calculated before substitution in Eq. (18). The motivation for the *ad-hoc* introduction of Eqs. (10) and (19) is to distinguish between the two regimes, of 2-D and 1-D detection that we observe experimentally. Figs. 3(a) and 3(b), for which $\hbar\omega = 3$ and 4.5 meV, respectively, both show that the assumption of a 1-D QPC density of states leads to a detector peak with an amplitude significantly smaller than G_0. (Note the higher background conductance for the smaller subband spacing of Fig. 3(a), since a larger number of 1-D subbands now contribute to the conductance. The same is true for the comparison of Figs. 3(c) and 3(d).) In Figs. 3(c) and 3(d), in contrast (for which $\hbar\omega = 1$ and 3 meV, respectively), the use of a 2-D detector density of states yields a peak amplitude much larger than G_0. In fact, the peak amplitudes exhibited in Figs. 3(a)–3(d) are in good agreement with our corresponding experimental observations in the 1-D and 2-D regimes (see Fig. 2). Notably, comparison of the data of Figs. 3(a) and 3(d), obtained for the same subband separations, shows that the peak amplitude is increased by a factor of around ten by the 2-D nature of the density of states.

To further understand the influence of the characteristics of the detector on the amplitude of its resonance, in Fig. 4, we break down the full resonance in terms of its contributions from the different QPC subbands. Fig. 4(a) is calculated from the data of Fig. 3(b), for which the 1-D subband separation is 4.5 meV. With a Fermi energy of 10 meV, and at zero temperature, one therefore expects that only the lowest two subbands should be populated. At 4.2 K, however, higher subbands should develop a non-zero population, and the results of Fig. 4(a) reflect these expectations. Considering the behavior away from the resonance condition (i.e., for $E_F - E_0 \neq 0$), the lowest two subbands are almost fully conducting, each with conductance (G_{pm}) close to G_0. The third mode is partially
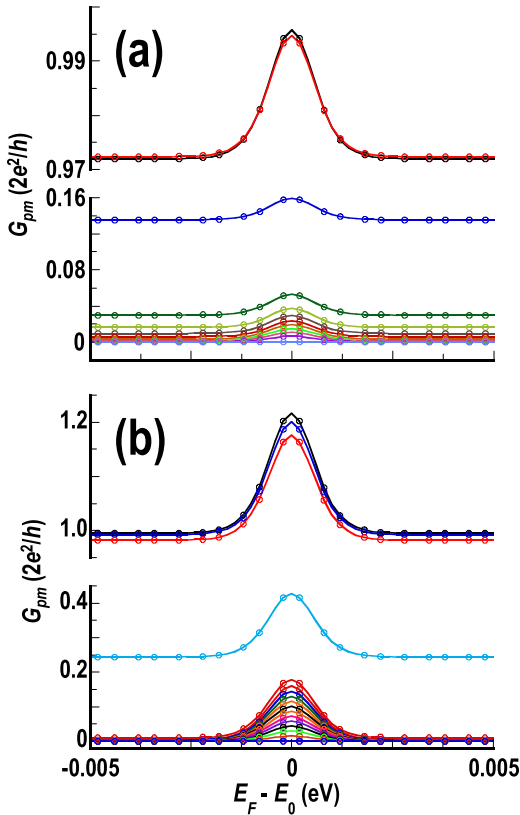
FIG. 4. (a) Contributions of the different subbands to the resonance of Fig. 3(b) ($\hbar\omega = 4.5$ meV). Conductance per mode (G_{pm}) is plotted on the vertical axis (note the break in this axis and the different scales before and after the break). The lowest two subbands are almost fully transmitted, while G_{pm} decreases systematically with increasing subband index. (b) Subband contributions (G_{pm}) for the resonance of Fig. 3(d) ($\hbar\omega = 3$ meV). Again note the break in the vertical axis and the different scales before and after this. The lowest three subbands are almost fully transmitted in this case, and G_{pm} decreases systematically for higher subbands.

VI. DISCUSSION AND CONCLUSIONS

The theoretical analysis of our experiments reveals a number of important aspects of the Fano resonance in the conductance of the detector-QPC. First, the results of Fig. 4 clearly show that, regardless of the detector dimensionality, this resonance is actually comprised of a set of simultaneous resonances, which arise individually from the coupling of *each* of the (fully- or partially-transmitted) detector subbands to the swept-QPC BS. Thus, the detector resonance should be viewed as a manifestation of the multi-continuum resonance predicted in the original work of Fano.[1] According to this interpretation, each subband serves as a unique continuum that gives rise to a Fano resonance due to its own, 2DEG-mediated, coupling to the BS. Second, our theory confirms the experimental observation (Fig. 2) that the resonance exhibited by the detector can significantly exceed G_0, when this QPC possesses a 2-D character. Essentially, the dependence of the resonance amplitude on the detector density of states arises from the fact that, in the 1-D case, the conductance of each subband is bounded by G_0, and the individual contributions of these subbands to the overall resonance are even smaller than this (Fig. 4(a)). No such restriction arises when the detector possesses a 2-D density of states, however, for which Fig. 4(b) shows that the contribution of the individual subbands is typically larger (although still somewhat smaller than G_0). After summing over all of these subbands, the resulting resonance can easily exceed G_0. An important feature revealed in Fig. 4 is that, even for modes that are only weakly conducting, their individual resonances can be significant (non-conductive subbands, on the other hand, do not contribute to the resonance at all).

While our theory for the integral-Fano formula captures key elements of the experiment, its success follows from an *ad-hoc* assumption that the detector supports a set of transverse subbands, to which we may assign either a one- or two-dimensional density of states. Since this approach is not strictly physically accurate, some justification for its introduction should be given, specifically in regards to the case that we refer to as "2-D" detection. This corresponds to the situation in which the detector QPC is either close to formation or in which it has just been formed. Under such conditions, the purely-2-D character of transport has been broken, but the 1-D subbands are not necessarily energetically well resolved. In this intermediate regime, *some* form of theoretical assumption is therefore required, and in our case, we impose this through the detector dimensionality. It should be noted that for the 1-D density of states, Eq. (10), the contribution of large energies is suppressed by a factor proportional to $E^{1/2}$. To introduce the same suppression for the 2-D case, we just formally insert the finite upper integration limit in Eq. (18). Ultimately, this approach can only be justified empirically, by its ability to account for the dramatic amplitude variations that we observe for the detector resonance in our experiments.

Another aspect of the comparison between experiment and theory concerns the symmetry of lineshape of the detector resonance. The resonances in Fig. 2 show an asymmetric character that is more pronounced in the 1-D regime of detection, consistent with our earlier studies.[16–19] The calculated peaks (Figs. 3 and 4), on the other hand, are much more symmetric (although not completely so). Most likely, this difference can be attributed to the fact that our theory

conducting, contributing $0.14G_0$, and the remaining modes provide an even smaller amount ($<0.1G_0$ in total). In combination, these contributions yield the observed background conductance of $2.14G_0$. Turning to the behavior at resonance, Fig. 4(a) shows that this also has contributions from all of the subbands that are at least partially conducting. While the largest of these come from the lowest two subbands, the higher ones also provide significant contributions, in spite of the fact that their background conductance $\ll G_0$. A similar picture is apparent in the results of Fig. 4(b), which break down the contributions to the 2-D resonance of Fig. 3(d). In this case, the subband separation is taken as 3.0 meV, so that the lowest three subbands are almost fully conducting. The fourth subband is partially conducting, contributing around $0.25G_0$, and with the contributions from even higher subbands included, we obtain the observed background conductance of close to $3.25G_0$. By summing the contributions at resonance, we ultimately obtain a resonance amplitude of around $1.75G_0$, consistent with Fig. 3(d).

accounts only for broadening due to electron transfer into and out of the detector QPC and the BS. In the experiment, however, other mechanisms can contribute to Γ and Γ_0, changing the q-parameter. Indeed, according to Eq. (13), an increase of Γ should lead to a decrease of q, and, correspondingly, to more asymmetric lineshape. Examination of specific scattering mechanisms (in particular electron-phonon and electron-electron interactions) and their influence on the lineshape are beyond the scope of this present paper and will need to be left for the future.

In conclusion, we have demonstrated that the Fano resonance exhibited by wavefunction-coupled QPCs can be viewed as a multi-continuum resonance, which arises from the coupling of the different conducting (or partially-conducting) modes of the detector to a common discrete state. In the case that we have referred to as 2-D detection, we have seen that, even though the individual mode contributions to the resonance are smaller than G_0, the net resonance can significantly exceed the conductance quantum. We therefore consider this giant Fano resonance as a characteristic signature of a multi-continuum process. In a notable difference with the original formulation of Fano,[1] our theory shows that the resonance width (Γ) and Fano parameter (q) are *not* constants of the system. Rather, they are involved in integrations over the electron energy in the detector and reservoirs, a result that we refer to as the "integral Fano formula." This "integral Fano formula" represents a new manifestation of Fano-resonance phenomenology, which could find broad application to mesoscopic systems, which tend to be much more strongly energy dependent than their atomic counterparts.

ACKNOWLEDGMENTS

[1]U. Fano, Phys. Rev. **124**, 1866 (1961).

[2]U. Fano and A. R. P. Rau, *Atomic Collisions and Spectra* (Academic, New York, 1986).

[3]J. P. Connerade, *Highly Excited Atoms* (Cambridge University Press, Cambridge, 1998).

[4]J. Faist, F. Capasso, C. Sirtori, K. W. West, and L. N. Pfeiffer, Nature (London) **390**, 589 (1997).

[5]M. Kroner, A. O. Govorov, S. Remi, B. Biedermann, S. Seidl, A. Badolato, P. M. Petrou, W. Zhang, R. Barbour, B. D. Gerardot, R. J. Warburton, and K. Karrai, Nature (London) **451**, 311 (2008).

[6]J. Göres, D. Goldhaber-Gordon, S. Heemeyer, M. A. Kastner, H. Shtrikman, D. Mahalu, and U. Meirav, Phys. Rev. B **62**, 2188 (2000).

[7]K. Kobayashi, H. Aikawa, S. Katsumoto, and Y. Iye, Phys. Rev. Lett. **88**, 256806 (2002).

[8]A. C. Johnson, C. M. Marcus, M. P. Hanson, and A. C. Gossard, Phys. Rev. Lett. **93**, 106803 (2004).

[9]A. E. Miroshnichenko, S. Flach, and Yu. S. Kivshar, Rev. Mod. Phys. **82**, 2257 (2010).

[10]A. R. P. Rau, Phys. Scr. **69**, C10 (2004).

[11]S. M. Cronenwett, H. J. Lynch, D. Goldhaber-Gordon, L. P. Kouwenhoven, C. M. Marcus, K. Hirose, N. S. Wingreen, and V. Umansky, Phys. Rev. Lett. **88**, 226805 (2002).

[12]T. Rejec and Y. Meir, Nature (London) **442**, 900 (2006).

[13]A. D. Güçlü, C. J. Umrigar, H. Jiang, and H. U. Baranger, Phys. Rev. B **80**, 201302(R) (2009).

[14]E. Welander, I. I. Yakimenko, and K.-F. Berggren, Phys. Rev. B **82**, 073307 (2010).

[15]T. Song and K.-H. Ahn, Phys. Rev. Lett. **106**, 057203 (2011).

[16]T. Morimoto, Y. Iwase, N. Aoki, T. Sasaki, Y. Ochiai, A. Shailos, J. P. Bird, M. P. Lilly, J. L. Reno, and J. A. Simmons, Appl. Phys. Lett. **82**, 3952 (2003).

[17]Y. Yoon, L. Mourokh, T. Morimoto, N. Aoki, Y. Ochiai, J. L. Reno, and J. P. Bird, Phys. Rev. Lett. **99**, 136805 (2007).

[18]Y. Yoon, M.-G. Kang, T. Morimoto, L. Mourokh, N. Aoki, J. L. Reno, J. P. Bird, and Y. Ochiai, Phys. Rev. B **79**, 121304(R) (2009).

[19]Y. Yoon, M.-G. Kang, P. Ivanushkin, L. Mourokh, T. Morimoto, N. Aoki, J. L. Reno, Y. Ochiai, and J. P. Bird, Appl. Phys. Lett. **94**, 213103 (2009).

[20]V. I. Puller, L. G. Mourokh, A. Shailos, and J. P. Bird, Phys. Rev. Lett. **92**, 96802 (2004).

[21]L. Mourokh, V. I. Puller, A. Yu. Smirnov, and J. P. Bird, Appl. Phys. Lett. **87**, 192501 (2005).

[22]Y. Yoon, M.-G. Kang, T. Morimoto, M. Kida, N. Aoki, J. L. Reno, Y. Ochiai, L. Mourokh, J. Fransson, and J. P. Bird, Phys. Rev. X **2**, 021003 (2012).

[23]S. Datta, *Electronic Transport in Mesoscopic Systems* (Cambridge University Press, 1995).

[24]D. K. Ferry, S. M. Goodnick, and J. P. Bird, *Transport in Nanostructures* (Cambridge University Press, 2009).

[25]V. Madhavan, W. Chen, T. Jamneala, M. F. Crommie, and N. S. Wingreen, Phys. Rev. B **64**, 165412 (2001).